ACS NANO

www.acsnano.org

ARTICLE

Stimuli-Responsive Actuator Fabricated by Dynamic Asymmetric Femtosecond Bessel Beam for *In Situ* Particle and Cell Manipulation

Rui Li,[§] Dongdong Jin,[§] Deng Pan, Shengyun Ji, Chen Xin, Guangli Liu, Shengying Fan, Hao Wu, Jiawen Li,* Yanlei Hu, Dong Wu,* Li Zhang,* and Jiaru Chu

Cite This: *ACS Nano* 2020, 14, 5233−5242

Read Online

ACCESS | Metrics & More | Article Recommendations | Supporting Information

ABSTRACT: Microscale intelligent actuators capable of sensitive and accurate manipulation under external stimuli hold great promise in various fields including precision sensors and biomedical devices. Current microactuators, however, are often limited to a multiple-step fabrication process and multimaterials. Here, a pH-triggered soft microactuator (<100 μm) with simple structure, one-step fabrication process, and single material is proposed, which is composed of deformable hydrogel microstructures fabricated by an asymmetric femtosecond Bessel beam. To further explore the swelling−shrinking mechanism, the hydrogel porosity difference between expansion and contraction states is investigated. In addition, by introducing the dynamic holographic processing and splicing processing method, more complex responsive microstructures (S-shaped, C-shaped, and tortile chiral structures) are rapidly fabricated, which exhibit tremendous expected deformation characteristics. Finally, as a proof of concept, a pH-responsive microgripper is fabricated for *in situ* capturing polystyrene (PS) particles and neural stem cells rapidly. This flexible, designable, and one-step approach manufacturing of intelligent actuator provides a versatile platform for micro-objects manipulation and drug delivery.

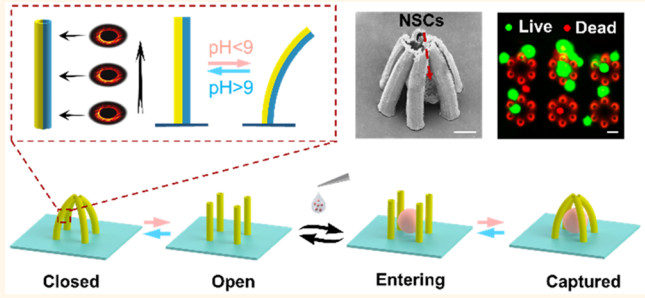

KEYWORDS: *microactuators, asymmetric femtosecond Bessel beam, porosity difference, pH-responsive microgripper, neural stem cells*

Microactuators are a type of device that can generate mechanical deformation under various forms of stimulations at the microscale.[1−3] Such feature greatly facilitates the potential applications of actuators in microrobotics,[4] tissue engineering,[5] and biomedical devices.[6] To make actuators intelligent, stimuli-responsive hydrogels have been widely adopted over the past decades of years. Stimuli-responsive hydrogels are kinds of hydrophilic polymers that swell and shrink when adapting to external environmental stimuli such as temperature,[7−9] pH,[10−13] light,[14] electric fields,[15] and so on.[16−18] On the basis of these hydrogels, many types of microactuators with favorable properties of intelligence and fast responses have been achieved by ultraviolet (UV) lithography.[19−23] For example, Seog et al. reported a chiral helical microactuator based on trilayer samples consisting of rigid plastic stripes sandwiching a temperature-responsive hydrogel.[19] Huang et al. developed magnetically powered microactuators with reconfigurable shape and controllable motility by photopatterning of magnetic hydrogel nanocomposites sequentially.[21] However, a multiple-step manufacturing process and multimaterials are usually involved in these fabrication methods, which are time-consuming and complicated.[22,23] Therefore, it is highly desirable for the development of microactuators with a facile manufacture method.

Compared to the traditional fabrication technology, femtosecond direct laser writing (fs-DLW) with the features of programmable exposure, true 3D processing ability, and high printing resolution[24,25] emerges as a more effective way as it can fabricate microactuator in a single-material and one-step manner. For instance, Zhang et al. and Hu et al. reported smart deformable microactuators by programming the size, distributions, and scan times of voxels at the nanoscale.[26,27] However, this fabrication technique is limited by its point-by-point scanning strategy, which leads to low processing efficiency. Various alternative schemes are developed to combat this

Received: January 15, 2020
Accepted: March 20, 2020
Published: March 20, 2020

https://dx.doi.org/10.1021/acsnano.0c00381
ACS Nano 2020, 14, 5233−5242

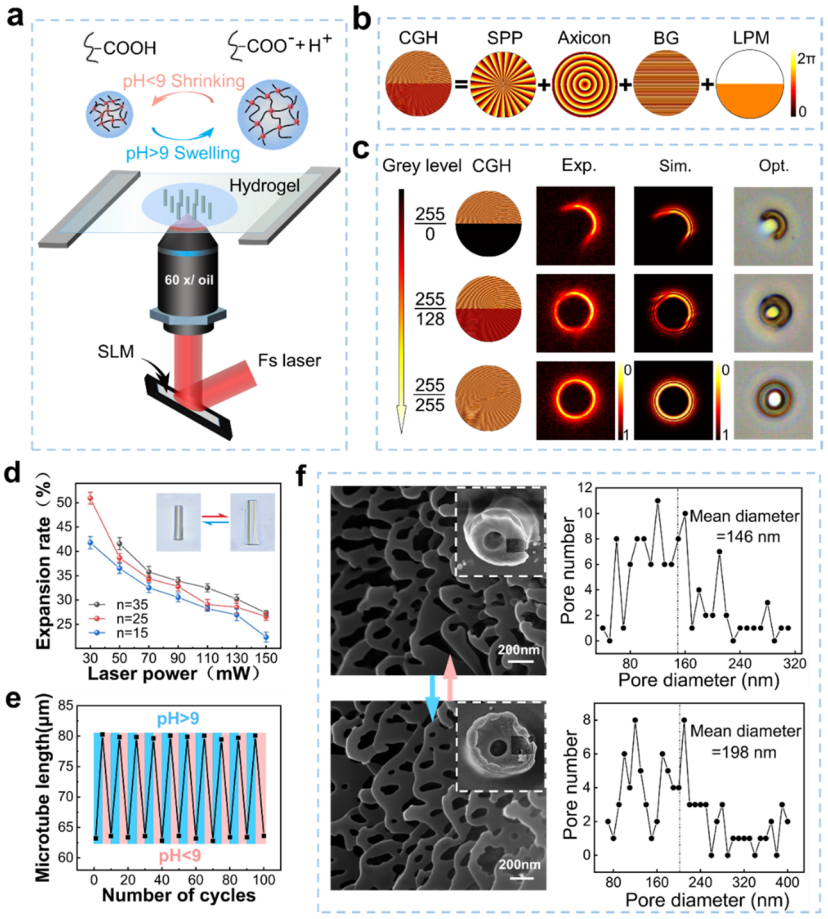

Figure 1. Holographic two-photon polymerization processing and the expansion and contraction properties of the pH-responsive hydrogel. (a) Rapid fabrication of pH-responsive microtubes based on local phase modulation of Bessel holograms, which are shrinking upon the pH changing below 9. (b) CGH is composed of spiral phase plate (topological charge n = 25), axicon radius (r_0 = 800 μm), blazed grating (Δ = 96 μm), and local phase modulation depth (gray level 255/150). (c) Experimental light field (the second line, Exp.) and simulational light field (the third line, Sim.) of Bessel beam with controllable energy distribution by partly tuning phase depths of holograms (the first row). The last line shows the optical micrographs (Opt.) of the ring microstructure processed by different holograms with different gray level. (d) Expansion rate of pH-responsive microtube decreases with the laser power and the topological charge n of the holograms increasing. (e) Cyclic reversible expansion−contraction behavior of the microtube as the solution pH is varied between >9 and <9. (f) Porosities of freeze-dried pH-responsive hydrogel, cut by focused ion beam (FIB), in contracted and expanded states.

problem. One method is to combine the spatial light modulation (SLM) technology with Fs-DLW systems to modulate the laser beam into diverse shapes, including a multiple beam spot array,[28] airy beams,[29] which produce complex 3D structures rapidly while keeping high resolution. Among these structured beams, Bessel beams have drawn extensive attention due to their nondiffracting and self-healing properties. Ring-shaped microtubes with different diameters have been fabricated using high-order Bessel beams.[30] What's more, by compressing the holograms phase depth, a ring light field with controllable intensity is utilized to process variable cross-section microtubes.[31] However, these modulation strategies can only produce ring structured light with symmetric energy distribution, and the local energy on the ring cannot be flexibly regulated, which results in limited fabrication capability. Moreover, these structured beams have not been used to fabricate responsive hydrogel-based micro-actuators.

Herein, we develop a local hologram phase modulation strategy that can generate an asymmetric ring structured femtosecond Bessel beam with nonuniform energy distribution, thus allowing fabrication of a pH-responsive hydrogel based microactuator in a single-material and one-step process much more rapidly than before. As our strategy generates a heterogeneous light field during the fabrication process and the pH-responsiveness of hydrogel is directly connected with the exposure laser power, a microtube with asymmetric swelling/shrinking property can be fabricated, which exhibits reversible bending and upright within 1 s when the solution pH value changes. The porosity difference between expansion and contraction states is further studied to clarify the responsive mechanism of the hydrogel. Moreover, we present a dynamic holographic processing method and splicing method to generate more complex pH-responsive microstructures (S-shaped, C-shaped microtubes and torsional chiral-structures) in about 10 s. Finally, an effective microgripper is demonstrated for trapping and releasing PS particles and neural stem cells. These microgrippers hold great promise for applications of micro-objects manipulation and studying single microparticle/cell behavior.

RESULTS AND DISCUSSION

Generation of Bessel Beam with Tunable Energy Distribution. The main principle of the SLM-based nano-

https://dx.doi.org/10.1021/acsnano.0c00381
ACS Nano 2020, 14, 5233−5242

fabrication system is schematically illustrated in Figure 1a. The liquid-crystal SLM is a pure phase modulator in the range of gray level (0−255), and 0 to 255 gray scale value represents 0 to 2π phase delay linearly on the hologram. After reflected from SLM, imprinted with the computer-generated-hologram (CGH), a Gaussian laser femtosecond beam (central wavelength λ = 800 *nm* with pulse repetition rate 80 MHz and pulse width 75 fs) can be modulated to a ring-structure Bessel beam.[30] As illustrated in Figure 1b, the CGH is composed of a spiral phase plate (SPP), an axicon, a blazed grating (BG), and a local phase modulation (LPM). The axicon generates a zeroth Bessel beam while the SPP converts the beam into the high order Bessel beam. The BG is an important part that separates the first-order light from others. Finally, the phase distribution of CGH without LPM can be expressed as

$$Ph_1(x_0, y_0) = mod(n\theta + 2\pi r/r_0 + 2\pi x_0/d, 2\pi) \quad (1)$$

where x_0 and y_0 are the horizontal axis and vertical axis in the Cartesian coordinate system on the SLM plane; n is the topological charge of SPP, which denotes the order of Bessel beam; $\theta = \tan^{-1}(y_0/x_0)$ is the polar angle and $r = \sqrt{x_0^2 + y_0^2}$ is the polar radius; r_0 is the radius of the axicon, and d is the period of the BG.

To regulate the light field intensity of the Bessel beam, an effective method has been adopted by just compressing the phase modulation depth.[31] The basic principle is shown as follows:

$$Ph_2(x_0, y_0) = mod(n\theta + 2\pi r/r_0 + 2\pi x_0/d, 2\pi) \times \varphi/2\pi \quad (2)$$

where $\varphi \in [0,2\pi]$ is the maximum phase modulation depth of the final hologram.

By varying φ from 0 to 2π, the diffraction efficiency η of the light spot of all orders can be changed correspondingly. Detailed formulas for calculation are given below:

$$n(\varphi) = 2 \times (1 - \cos\varphi)/(\varphi - 2n\pi)^2 \quad (3)$$

However, this strategy can only generate a ring-structure Bessel beam with uniform intensity and cannot modulate the local energy distribution of the Bessel beam flexibly. To resolve this problem, we develop a strategy by superimposing a LPM on the hologram as shown in Figure 1b. In theory, any part of the ring-structure light field can be modulated depending on the shape and phase modulation depth of the LPM (Figure S1, Supporting Information). Here, a semicircle is chosen as representative shape of LPM to divide the hologram into two equal parts. One part (white) means the phase distribution staying unchanged, while the other part (orange) means that the phase modulation depth is φ of the LPM. Finally, the phase profile of superimposed hologram is shown as follows:

$$Ph_3(x_0, y_0) = \begin{cases} mod(n\theta + 2\pi r/r_0 + 2\pi x_0/d, 2\pi), & t < 0 \\ mod(n\theta + 2\pi r/r_0 + 2\pi x_0/d, 2\pi) \times \varphi/2\pi, & t > 0 \end{cases} \quad (4)$$

where $t = x_0 \cos\alpha + y_0 \sin\alpha$ and $\alpha \in [0, 2\pi]$ is the angle between boundary of the LPM and the horizontal axis of the hologram (Figure S2, Supporting Information).

After reflected by the SLM, the modulated Bessel beam is focused into pH-responsive hydrogel by an oil-immersion objective lens (60×, NA = 1.35). Simulated and experimental light field modulated by different holograms is illustrated in Figure 1c to show the principle of the local phase modulation and the controllable energy distribution of the Bessel beam. The three holograms are the same except the maximum gray scale value of the LPM, which are 0, 128, and 255 from top to bottom representing the phase modulation depth of 0,π and 2π, correspondingly. It can be seen that the experimental results have a good consistency with the simulation calculation. Therefore, a ring-shaped Bessel beam with controllable energy distribution can be generated by superimposing a LPM onto the holograms. The shape of the LPM and phase modulation depth determine the energy distribution and energy intensity of a ring Bessel light field, respectively.

Expansion and Shrinkage Mechanism of pH-Responsive Hydrogel. The pH-responsive hydrogel adopted here is a poly(acrylic acid) (pAAc)-based hydrogel with a large amount of carboxyl in the side chain (Figure 1a).[32] At high pH value, these carboxyl groups become deprotonated and negatively charged, which will generate electrostatic repulsion forces between molecular chains, resulting in significant expansion of the hydrogel network. Inversely, the network collapses when the carboxyl groups are protonated at low pH and the hydrogel is shrinking.[33] In our work, the fabricated hydrogel structure will swell or shrink at a critical pH value of ∼9, and all the swelling and shrinking process generally finish within 1 s, mainly due to the fast diffusion rate of ions in hydrogel matrix at small scale.

To investigate the pH-responsive properties of the material, we perform a laser power-dependent swelling rate analysis of the hydrogel microtube fabricated by focused uniform Bessel beam (255/255 in Figure 1c). We define a swelling rate to quantitatively evaluate the deformation capability of hydrogel microtubes:

$$\varepsilon\ (\%) = (l_1 - l_0)/l_0 \times 100 \quad (5)$$

where l_1 and l_0 are the length of expanded and shrunken microtubes. Figure 1d shows the expansion rate of the microtubes with different diameters modulated by holograms with different topological charge (n = 15, 25, 35), while r_0 keeps the same (r_0 = 800). The expansion rate decreases from 51% to 26% with the laser power increasing from 30 mW to 150 mW, as the higher exposure laser power makes the cross-linking degree greater, which subsequently limits the deformation capability of hydrogel.

Figure 1e depicts the length of microtubes for multiple cycles of stimulation. Furthermore, to gain a deeper insight into the pH-induced swelling mechanism of the hydrogel, we explore the porosities of photopolymerized pH-responsive hydrogel both in expanded and collapsed states (Figure 1f). After fabricated by focused Bessel beam and then developed, two identical samples with hydrogel microtube arrays are soaked in DI water (pH = 7) and ammonium hydroxide (NH_4OH) solution (pH = 14), respectively. Afterward, to keep their original states (contracted and expanded) in solution, we adopt a freeze-drying method. After cut by focused ion beam (FIB), field-emission SEM images (Figure 1f) indicate the inner pore structure of hydrogel microtubes in contracted and expanded states. By outlining the pores of hydrogel in ImageJ software, we obtain the mean diameters of the pores in two states, which can represent the porosities of hydrogel microtubes (for details see Figure S3 in Supporting Information). Figure 1f shows that the mean diameter has a 35.6% increase from shrinking state (146 nm) to swelling state

https://dx.doi.org/10.1021/acsnano.0c00381
ACS Nano 2020, 14, 5233−5242

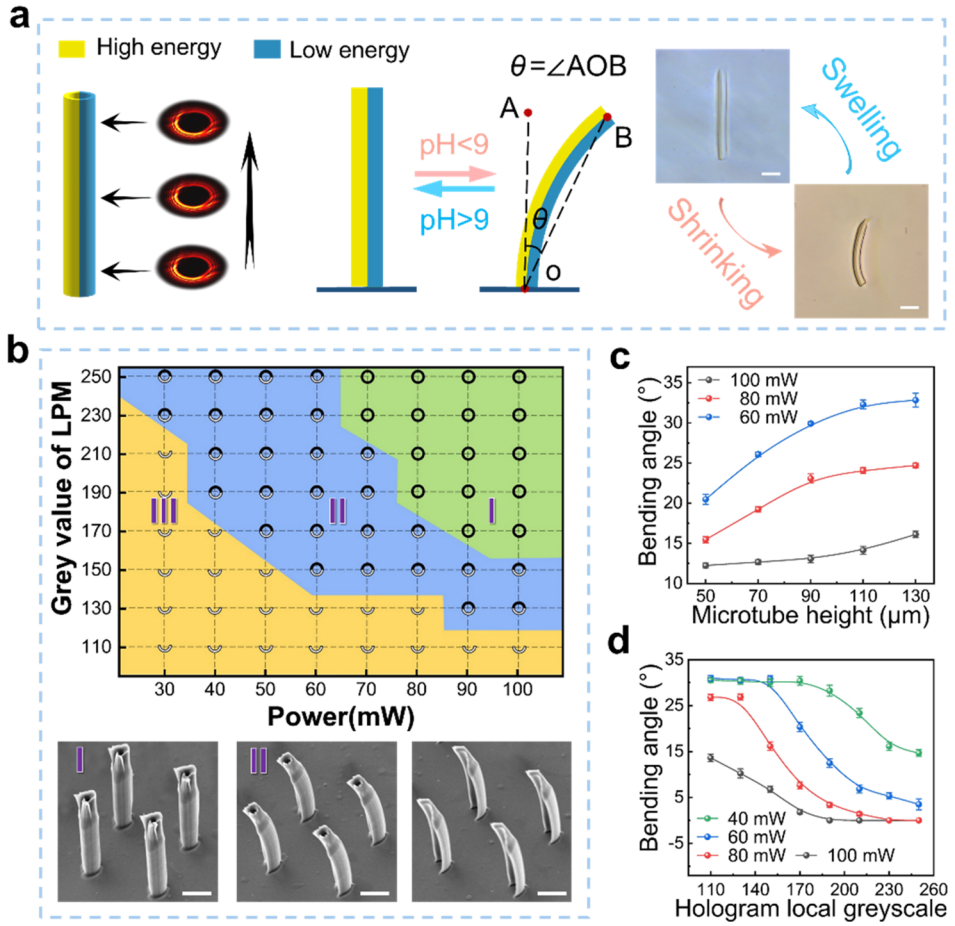

Figure 2. Schematic diagram of bended pH-triggered microtubes with different bending angles. (a) Bendable microtubes processing strategies by local modulated Bessel beam. The diagrammatic sketch and observation of expnsion and contraction of microtubes are showed in the middle and right side, respectively. (b) Dependency map of three types of microtubes (I, II, III) on laser power and local gray value of hologram. Scale bars: 20 μm. (c, d) Bending angles of microtubes are effected by height of microtube, laser power and local gray level of hologram. Different line colors stand for different laser power. All scale bar: 20 μm.

(198 nm), and these data are consisted with the swelling rate (ε). To the best of our knowledge, the different porosities of stimulus-responsive hydrogel (swelling/shrinking states) fabricated by two-photon polymerization have not been reported before.

Fabrication of Polymorphic pH-Triggered Microtubes. Since the expansion rate of the pH-responsive hydrogel is determined by processing energy, the microtubes can be induced to multiple shapes by controlling the power of laser source and the phase modulation depth of Bessel holograms. A LPM is superimposed on the hologram to modulate a ring-structure Bessel beam with heterogeneous intensity distribution, which is a combination of a high-energy semicircular and a low-energy semicircular. Straight heteromicrotubes fabricated by locally modulated beam can shrink into bended microtubes by changing pH value of the aqueous environment (schematically illustrated in Figure 2a) (Video S1, Supporting Information).

Besides, various combinations of heterogeneous energy distribution of Bessel beam can be realized by tuning the power of laser source (30−100 mW) and the local gray scale values of holograms (110−250, Figure 2d). The graph is divided into three regions corresponding to three types of pH-responsive microtubes (I, II, III). The green region (type I) shows negligible pH-responsive bending since the total laser power is too high and the heterodistribution of light field is not significant. Inversely, semicircle-shaped microtubes have been fabricated, illustrated in the orange area (type III). This is because the power of the locally modulated semicircle beam is lower than the exposure threshold. With moderate power of laser source and proper gray level of partial holograms, pH-induced bendable microtubes (type II, blue area) can be obtained. Hence, the shapes of type II and type III transform from straight to bended microtubes as the pH value in solution falls below 9.

Furthermore, to explore the stimuli-responsive bending behavior of the heteromicrotubes, three essential parameters are chosen in the hydrogel microtubes processing, namely the height of microtubes (h), the local gray value of holograms (g), and the power of laser source (p). A bending angle (θ) can quantificationally describe the bending degree, which is defined as

$$\theta = \arcsin(\delta/h) \tag{6}$$

where δ is the horizontal distance between the tip point and the root of the microtube, and h is the height of microtube. Detailed statistics about the bending angle of pH-responsive microtubes are shown in Figure 2c and d. We conclude that the bending degree is positively related to the height of microtube while inversely proportional to total energy and

https://dx.doi.org/10.1021/acsnano.0c00381
ACS Nano 2020, 14, 5233−5242

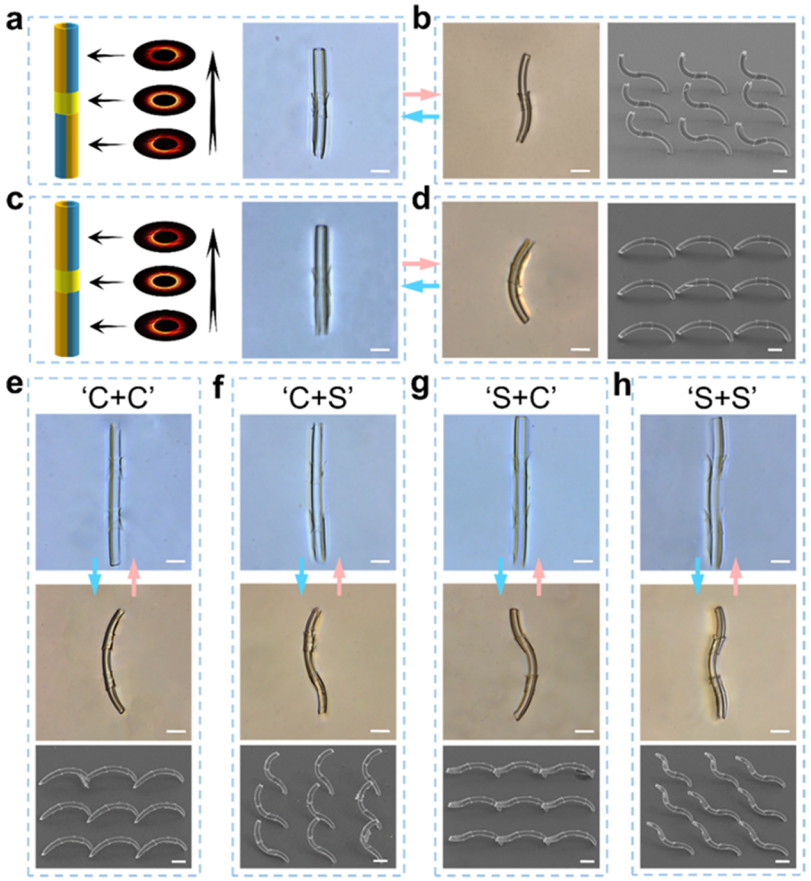

Figure 3. Shape deformation of stimuli-responsive multisegment microtubes. (a–d) Processing method of S-shaped and C-shaped microtubes, which are straight when the solution pH values are over 9. The right-hand side images show the SEM of supercritical dried structures. (e–h) Three-segment microtubes, which can shrink into different shapes. The bottom row images show the SEM of supercritical dried structure. The lengths of all the microtubes are designed to be 160 μm. The low power (blue) is 30 mW, middle power (orange) is 60 mW, and high power (yellow) is 100 mW. All SEM images are taken in contracted state. All scale bars: 20 μm.

local greyscale of hologram. In short, moderate total processing energy (60–80 mW), higher height of microtube, and not particularly low gray value of local phase of hologram (>130) are needed in the fabrication of pH-responsive microtubes, which show distinct bending at low pH.

Dynamic Holographic Processing of Designed Multisegment-Shaped Microtubes. To achieve more sophisticated and diverse response shapes, we adopt dynamic holographic processing strategy to fabricate multisegment deformable microtubes. In the above, the hydrogel sample is fixed on piezoelectric platform and the ring-structure beam is focused in it. A microtube is fabricated when the platform moves along the Z direction. However, this processing strategy can only fabricate microtubes that only bend to one direction, which is a bit limited. A dynamic holographic processing method can address this problem properly by continuously varying the holograms displayed on the SLM, and in the meantime, the piezoelectric platform moves along the Z direction; hence, multisegment heteromicrotubes can bend into complex shapes when responding to the environment.

An S-shaped microtube is designed and fabricated as a response to the external stimulus just as shown in Figure 3a and b. The processing energy are color-coded, and the color changing from blue, to orange, to yellow indicates increasing exposure energy and thus decreasing swelling capacity. The microtube is polymerized by three types of Bessel beam, in which the energy distribution is opposite in the upper and lower section, while the middle part is a symmetrical beam with no phase modulation. By decreasing the pH value below 9, the upper section bends to the right side, while the lower section bends to the left side, leading to a straight microtube (swelled) that becomes an S-shaped actuation pattern (shrunk) (Video S2, Supporting Information). We design the middle section as a yielding point to transform the bending direction; otherwise, the upper and lower section will only bend to a same direction (Figure S4, Supporting Information). In addition, a C-shaped microtube can be easily designed by keeping upper and lower sections the same, which will both bend to right side when shrinking, shown in Figure 3c and d and Video S3 (Supporting Information).

To achieve more complex shapes, more yielding points are introduced into our structures. Figure 3e–h show that three-segment microtubes with two middle sections shrink into different shapes (Video S4, Supporting Information). These examples demonstrate that our dynamic holographic processing combined with local phase modulation strategy can fabricate multisegment heteromicrotubes with precisely controlled exposure dose distribution, which exhibit complex shapes after responding to environmental stimulus.

Rapid Processing of Torsional Chiral Responsive-Structure. In addition to conventional bending, torsion of the hydrogel microstructures is also realized by splicing processing method to achieve more freedom of motions. Here, we mainly adopt a semicircular microtube photopolymerized by semiring

https://dx.doi.org/10.1021/acsnano.0c00381
ACS Nano 2020, 14, 5233–5242

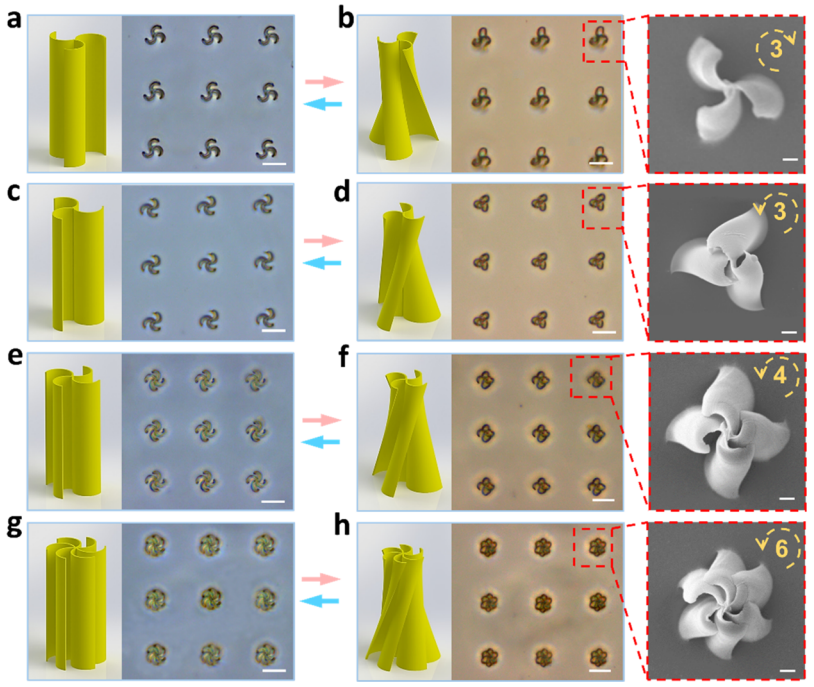

Figure 4. pH-responsive multivalve torsional chiral structure processed by multistep splicing. Torsional trivalve (a, b) left-chiral and (c, d) right-chiral microstructures spliced by three semimicrotubes, fabricated by semicircular light field three times. Scale bars: 20 μm. (e−h) Four-valve and six-valve tortile right-handed microstructures spliced by four and six semimicrotubes, respectively. Scale bars: 20 μm. The height all microstructures are 45 μm; laser power is 60 mW. The right side images illustrate the SEM of supercritical dried structures. All SEM images are taken in contracted state. Scale bars: 2 μm.

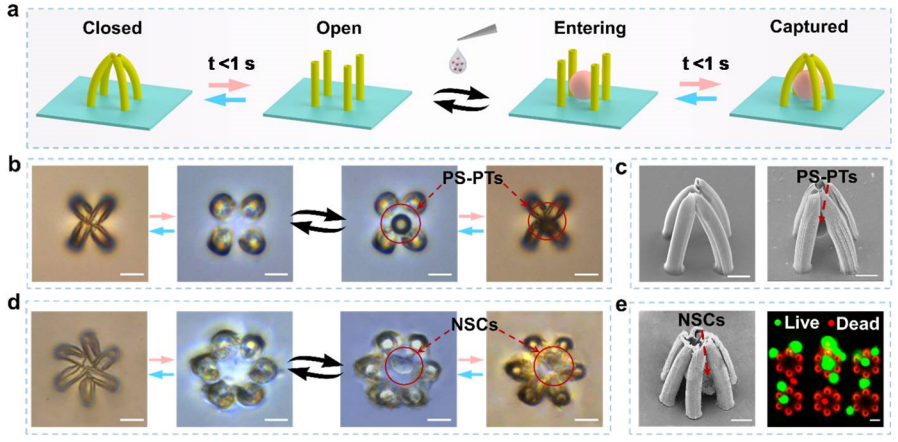

Figure 5. pH-responsive microparticle and cell gripper. (a) Schematic illustration of actuator with four fingers, which is closed when shrinking and open when swelling. After dropping the deionized water solution mixed with PS beads on the sample, the open trapper catches the PS particle, which can be washed away by DI water. Only when closed, the PS particle is captured tightly. (b) Experimental diagram of 4-finger microgripper and PS particles (PS−PTs, 13 μm) capture process. The length of each finger is 60 μm and distance between adjacent fingers is 20 μm. Scale bar: 20 μm. (c) SEM images of the gripper without/with particles. Scale bar: 10 μm. (d) Experimental diagram of 6-finger cell microgripper and cell capture process. The distance between adjacent fingers is 18 μm. Scale bar: 20 μm. (e) SEM of the microgripper with cell inside in contracted state and cell living and dead dyeing experiment. Green stands for live while red (solid) stands dead, red (hollow) stands for microgripper. All scale bars: 10 μm.

Bessel beam (Figure 1c, 255/0) to process torsional chiral responsive-structure. A single semiring microtube bends in the gap direction (normal direction perpendicular to the vertical section, shown in Figure S2, Supporting Information) as a response to the pH of solution. By changing the boundary direction (perpendicular to borderline of the local phase modulation area in hologram) from 0 to 2π, the gap direction varies nonlinearly. A detailed corresponding relation is illustrated in Figure S2, Supporting Information.

Interestingly, if three semicircular microtubes with different gap direction (angle 60°) splice together with the same side, a left-chiral structure is obtained (Figure 4a), which exhibits chiral torsion when the solution pH < 9 (Figure 4b, Video S5, Supporting Information) because during its shrinking time, the center part of the microstructure is restricted and stays straight, while the edge side is free and shrinks with bending. Conversely, the twisting direction is reversed by changing the semicircular microtubes with inverse gap direction (Figure

https://dx.doi.org/10.1021/acsnano.0c00381
ACS Nano 2020, 14, 5233−5242

4c,d). Finally, to perform more sophisticated actuations, we fabricate multivalve chiral structures with four and six semicircular microtubes (Figure 4e−h, Video S6, Supporting Information).

It is worth noting that the height of microstructure has a significant influence on its morphology. The height of all structures here is set to 45 μm, which is determined by speed (v) and exposure time (t). By increasing the exposure time while keeping the speed unchanged (30 μm/s), we can control the structure height flexibly. However, if the structure is too high (>90 μm), microtubes will separate from each other (for details see Figure S5 in Supporting Information). Thus, we keep the height under 60 μm to get better chiral structure.

Responsive Microgripper to Capture PS Particle and Single Cell *In Situ*. Recently, various studies on micro/nanoscale stimuli-responsive actuators have been carried out for the applications of microparticles manipulation[34] and cells capture.[6,35] We develop a pH stimuli-responsive actuator constituted by our bendable hydrogel microtubes, which can be used to trap microparticles and single cells *in situ*. The actuator has a resolution up to 300 nm depending on the diameter of the ring Bessel beam, and the maximum size is 200 μm × 200 μm × 200 μm, which is determined by the moving range of the nanopositioning stage.

The microgripper processing method is illustrated in Figure 5a. This device is composed of four microtubes as fingers, which are straight when swelling (open state) while bending to the same point after shrinking (closed state). Every microtube has a diameter of 10 μm and a height of 60 μm, and the distance between adjacent microtubes is 20 μm to match the size of PS particle. The laser power is 60 mW, and the local gray value of holograms is 150. To demonstrate the particles capture ability of our actuators, we prepare PS microspheres solution (13 μm diameter, 10 vol.%) and then drop it on the open microstructures. Figure 5b depicts that the actuator has captured a single PS microparticle. Then dilute acid solution (pH < 7) is added, and our gripper is folded to hold the particles from being washed away. Afterward, we drop enough dilute alkali solution (pH > 9) and the gripper unfolds with particle coming out, which can be easily washed away. Therefore, the pH-responsive gripper possesses microspheres capturing and releasing ability within a second when responding to environmental conditions (Video S7, Supporting Information). Additionally, by changing the distance of adjacent microtubes and the height of microtubes, our actuator can capture a microsphere with different diameters.

Besides capturing microparticles, our microgripper can capture a single cell. A six-finger microgripper is fabricated to increase the possibility to capture cells for enlarged room in each gripper and avert the risk of the cell escaping from the interspace between two adjacent microtubes. To prevent the cell from death or dangerous mutations, the microgripper is in its swelling state (open) initially (Figure 5d). Then cell medium with NE-4C neural stem cell is dropped on these trappers. The distance between adjacent fingers is 18 μm and the diameter of the middle space is 20 μm, and the cells are smaller with the diameter of 10−15 μm (Figure S6, Supporting Information). Until the cell sinks and is fallen into the trapper, dilute hydrochloric acid (pH < 7) is added immediately to modulate the solution to neutral (pH = 7), making the trapper closed and the cell captured. Notably, this operation can be finished within 1 min. A 2 × 2 array of 6-finger cell microgrippers is fabricated to show that the gripper can capture multiple particles at the same time (Figure S7, Supporting Information). Live and dead cell assay is carried out on the following day to identify the cell states. As shown in Figure 5e, the green, red (solid), and red (hollow) colors represent the alive cells, dead cells, and hydrogel microgripper, respectively. About 75% cell survival rate at the second day explains that our pH-triggered catching experiment does little harm to the cells. Finally, a SEM image of the microgripper with cell captured inside in contracted state is demonstrated. As a proof of concept, this rapid cell microgripper offers a method to cell manipulation. Since the microgripper is a polymeric actuator, further efforts need to be paid to broaden the applications, for example, integrated circuit[36] and optical imaging,[37] by femtosecond laser-induced reduction of metal on the hydrogel.[38,39] Besides, future studies will aim to investigate the holographic method to generated light field of arbitrary geometry instead of ring structured Bessel beam, and more complex actuators can be fabricated.

CONCLUSION

In summary, a density distribution controllable femtosecond Bessel beam is generated by locally compressing the phase modulation depth of the hologram. On the basis of this asymmetric beam, a pH-responsive microactuator composed of bendable hydrogel microtubes has been successfully fabricated. Composed with conventional microactuators, this actuator demonstrates a facile manufacture method, single material and one-step fabrication processing. To further study the expansion and contraction mechanism of the microtube, the hydrogel porosity difference in swelling (198 nm) and shrinking (146 nm) states is reported. In addition, by introducing dynamic holographic processing method and splicing processing method, S-shaped, C-shaped, multisegment microtubes, and multivalve torsional chiral structures are obtained and can realize tremendous deformation capacities. Finally, as a proof of concept, we fabricate multifinger responsive microgrippers to capture PS microparticles and neural stem cells, which have potential applications in microobjects manipulation and drug delivery. It is believable that, with the rapid development of smart materials, our pH-responsive microactuator may find broad applications, for example, in the integrated circuit and optical imaging field.

EXPERIMENTAL SECTION

Preparation of pH-Responsive Hydrogel. First, 1.6 g of *N*-isopropylacrylamide (NIPAAm, 98%), 0.8 mL of acrylic acid (AAc, 99%), and 0.15 g of polyvinylpyrrolidone (PVP, average Mw ≈ 1 300 000) were added to 1 mL of ethyl lactate (EL, 98%) and then stirred vigorously. Then 2.5 mL of the above solution, 0.5 mL of dipentaerythritol hexaacrylate (DPEHA,98%), 0.5 mL of triethanolamine (TEA, 99%), and 100 μL of 4,4-bis(diethylamino) benzophenone (EMK, 97%)/*N*,*N*-dimethylformamide (DMF, 99.5%) solution (20 wt.%) were mixed, followed by stirring 12 h, to mix each component completely. Finally, the precursor was kept in yellow light condition to avoid unnecessary light exposure.

Coverslips Functionalization. Round glass coverslips (diameter = 22 mm) were cleaned and sonicated with acetone and 2-propanol for 30 min. A solution of 0.5% TPM in 100 mL of ethanol was prepared. Then 3 mL of acetic acid (1:10 in Milli-Q water) was added, and the coverslips were immersed in

https://dx.doi.org/10.1021/acsnano.0c00381
ACS Nano 2020, 14, 5233−5242

the final solution for 5 min. Afterward, the coverslips were rinsed with absolute ethanol and dried with nitrogen.

Preparation of PS Particles and Cells. PS particles with diameters of 13 μm were mixed in deionized water with volume ratio 1:10, followed by 10 min of ultrasonic mixing, and the final PS volume concentration was 10%.

ASSOCIATED CONTENT

Supporting Information

The Supporting Information is available free of charge at https://pubs.acs.org/doi/10.1021/acsnano.0c00381.

Figures of modulated light field, hydrogel poriosities, gap direction and boundary direction, PS particles and cells, charity microstructure with different height, microtubes with different diameters, and array of microgrippers (PDF)

Swelling and shrinking deformation process of bendable microtubes (MP4)

Swelling and shrinking deformation process of S-shaped microtubes (MP4)

Swelling and shrinking deformation process of C-shaped microtubes (MP4)

Three-segment microtubes have shrunk into 'C+C', 'S +S', 'C+S', and 'S+C' shapes (MP4)

Twist process of trivalve left- and right-charity micro-structures (MP4)

Twist process of four-valve and six-valve right-handed microstructures (MP4)

Trapping and releasing process of PS microparticle using pH-responsive microgripper (MP4)

AUTHOR INFORMATION

Corresponding Authors

Jiawen Li − *Key Laboratory of Precision Scientific Instrumentation of Anhui Higher Education Institutes, CAS Key Laboratory of Mechanical Behavior and Design of Materials, Department of Precision Machinery and Precision Instrumentation, University of Science and Technology of China, Hefei 230026, China;* orcid.org/0000-0003-3950-6212; Email: jwl@ustc.edu.cn

Dong Wu − *Key Laboratory of Precision Scientific Instrumentation of Anhui Higher Education Institutes, CAS Key Laboratory of Mechanical Behavior and Design of Materials, Department of Precision Machinery and Precision Instrumentation, University of Science and Technology of China, Hefei 230026, China;* orcid.org/0000-0003-0623-1515; Email: dongwu@ustc.edu.cn

Li Zhang − *Department of Mechanical and Automation Engineering, The Chinese University of Hong Kong, Hong Kong 999077, China;* orcid.org/0000-0003-1152-8962; Email: lizhang@mae.cuhk.edu.hk

Authors

Rui Li − *Key Laboratory of Precision Scientific Instrumentation of Anhui Higher Education Institutes, CAS Key Laboratory of Mechanical Behavior and Design of Materials, Department of Precision Machinery and Precision Instrumentation, University of Science and Technology of China, Hefei 230026, China*

Dongdong Jin − *Department of Mechanical and Automation Engineering, The Chinese University of Hong Kong, Hong Kong 999077, China;* orcid.org/0000-0003-4833-538X

Deng Pan − *Key Laboratory of Precision Scientific Instrumentation of Anhui Higher Education Institutes, CAS Key Laboratory of Mechanical Behavior and Design of Materials, Department of Precision Machinery and Precision Instrumentation, University of Science and Technology of China, Hefei 230026, China*

Shengyun Ji − *Key Laboratory of Precision Scientific Instrumentation of Anhui Higher Education Institutes, CAS Key Laboratory of Mechanical Behavior and Design of Materials, Department of Precision Machinery and Precision Instrumentation, University of Science and Technology of China, Hefei 230026, China*

Chen Xin − *Key Laboratory of Precision Scientific Instrumentation of Anhui Higher Education Institutes, CAS Key Laboratory of Mechanical Behavior and Design of Materials, Department of Precision Machinery and Precision Instrumentation, University of Science and Technology of China, Hefei 230026, China*

Guangli Liu − *Key Laboratory of Precision Scientific Instrumentation of Anhui Higher Education Institutes, CAS Key Laboratory of Mechanical Behavior and Design of Materials, Department of Precision Machinery and Precision Instrumentation, University of Science and Technology of China, Hefei 230026, China;* orcid.org/0000-0001-7361-7907

Shengying Fan − *Key Laboratory of Precision Scientific Instrumentation of Anhui Higher Education Institutes, CAS Key Laboratory of Mechanical Behavior and Design of Materials, Department of Precision Machinery and Precision Instrumentation, University of Science and Technology of China, Hefei 230026, China*

Hao Wu − *Key Laboratory of Precision Scientific Instrumentation of Anhui Higher Education Institutes, CAS Key Laboratory of Mechanical Behavior and Design of Materials, Department of Precision Machinery and Precision Instrumentation, University of Science and Technology of China, Hefei 230026, China*

Yanlei Hu − *Key Laboratory of Precision Scientific Instrumentation of Anhui Higher Education Institutes, CAS Key Laboratory of Mechanical Behavior and Design of Materials, Department of Precision Machinery and Precision Instrumentation, University of Science and Technology of China, Hefei 230026, China;* orcid.org/0000-0003-1964-0043

Jiaru Chu − *Key Laboratory of Precision Scientific Instrumentation of Anhui Higher Education Institutes, CAS Key Laboratory of Mechanical Behavior and Design of Materials, Department of Precision Machinery and Precision Instrumentation, University of Science and Technology of China, Hefei 230026, China;* orcid.org/0000-0001-6472-8103

Complete contact information is available at: https://pubs.acs.org/10.1021/acsnano.0c00381

Author Contributions

[§]R.L. and D.J. contributed equally to this paper. R.L., J.W.L., and D.W. designed the experiment. D.D.J. made the pH-responsive materials. R.L., D.P., and S.Y.J. fabricated samples. R.L. and G.L.L. performed freeze-drying experiment. R.L. and S.Y.F. conducted the cell capturing experimnt. R.L., C.X., and H.W. analyzed the data and prepared the manuscript. Y.L.H., W.D., J.W.L., L.Z., and J.R.C reviewed and revised the paper.

Notes

The authors declare no competing financial interest.

https://dx.doi.org/10.1021/acsnano.0c00381
ACS Nano 2020, 14, 5233−5242

ACKNOWLEDGMENTS

This work is supported by the National Key R&D Program of China (2018YFB1105400), National Natural Science Foundation of China (Nos. 51675503, 51875544, 61805230, 51805509), Aeronautical Science Fund (2018ZE78004), Fundamental Research Funds for the Central Universities (WK2090000013, WK2090090021, WK6030000131, WK6030000103), Youth Innovation Promotion Association CAS (2017495), and Foundation of Equipment Development Department (6220914010901). We acknowledge the Experimental Center of Engineering and Material Sciences at USTC for the fabrication and measuring of samples. This work was partly carried out at the USTC Center for Micro and Nanoscale Research and Fabrication.

REFERENCES

(1) Ionov, L. Polymeric Actuators. *Langmuir* **2015**, *31*, 5015−5024.
(2) Wu, T.; Nieminen, T. A.; Mohanty, S.; Miotke, J.; Meyer, R. L.; Rubinsztein-Dunlop, H.; Berns, M. W. A Photon-Driven Micromotor Can Direct Nerve Fibre Growth. *Nat. Photonics* **2012**, *6*, 62−67.
(3) Silverberg, J. L.; Na, J.-H.; Evans, A. A.; Liu, B.; Hull, T. C.; Santangelo, C. D.; Lang, R. J.; Hayward, R. C.; Cohen, I. Origami Structures with a Critical Transition to Bistability Arising from Hidden Degrees of Freedom. *Nat. Mater.* **2015**, *14*, 389−393.
(4) Huang, H. W.; Uslu, F. E.; Katsamba, P.; Lauga, E.; Sakar, M.; Nelson, B. Adaptive Locomotion of Artificial Microswimmers. *Sci. Adv.* **2019**, *5*, eaau1532.
(5) Drury, J. L.; Mooney, D. J. Hydrogels for Tissue Engineering: Scaffold Design Variables and Applications. *Biomaterials* **2003**, *24*, 4337−4351.
(6) Breger, J. C.; Yoon, C.; Xiao, R.; Kwag, H. R.; Wang, M. O.; Fisher, J. P.; Nguyen, T. D.; Gracias, D. H. Self-Folding Thermo-Magnetically Responsive Soft Microgrippers. *ACS Appl. Mater. Interfaces* **2015**, *7*, 3398−3405.
(7) Yoshida, R.; Uchida, K.; Kaneko, Y.; Sakai, K.; Kikuchi, A.; Sakurai, Y.; Okano, T. Comb-Type Grafted Hydrogels with Rapid Deswelling Response to Temperature Changes. *Nature* **1995**, *374*, 240−242.
(8) Hu, Z. B.; Chen, Y. Y.; Wang, C. J.; Zheng, Y. D.; Li, Y. Polymer Gels with Engineered Environmentally Responsive Surface Patterns. *Nature* **1998**, *393*, 149−152.
(9) Zarzar, L. D.; Kim, P.; Kolle, M.; Brinker, C. J.; Aizenberg, J.; Kaehr, B. Direct Writing and Actuation of Three-Dimensionally Patterned Hydrogel Pads on Micropillar Supports. *Angew. Chem., Int. Ed.* **2011**, *50*, 9356−9360.
(10) Dong, L.; Jiang, H. Autonomous Microfluidics with Stimuli-Responsive Hydrogels. *Soft Matter* **2007**, *3*, 1223−1230.
(11) Qu, J. B.; Chu, L. Y.; Yang, M.; Xie, R.; Hu, L.; Chen, W. M. A pH-Responsive Gating Membrane System with Pumping Effects for Improved Controlled Release. *Adv. Funct. Mater.* **2006**, *16*, 1865−1872.
(12) Zhang, J.; Xie, R.; Zhang, S. B.; Cheng, C. J.; Ju, X. J.; Chu, L. Y. Rapid pH/Temperature-Responsive Cationic Hydrogels with Dual Stimuli-Sensitive Grafted Side Chains. *Polymer* **2009**, *50*, 2516−2525.
(13) Zhang, J.; Chu, L. Y.; Li, Y. K.; Lee, Y. M. Dual Thermo- and pH-Sensitive Poly(*N*-Isopropylacrylamide-Co-Acrylic Acid) Hydrogels with Rapid Response Behaviors. *Polymer* **2007**, *48*, 1718−1728.
(14) Li, W.; Wang, J.; Ren, J.; Qu, X. 3D Graphene Oxide-Polymer Hydrogel: Near-Infrared Light-Triggered Active Scaffold for Reversible Cell Capture and On-Demand Release. *Adv. Mater.* **2013**, *25*, 6737−6743.
(15) Morales, D.; Palleau, E.; Dickey, M. D.; Velev, O. D. Electro-Actuated Hydrogel Walkers with Dual Responsive Legs. *Soft Matter* **2014**, *10*, 1337−1348.
(16) Satarkar, N. S.; Hilt, J. Z. Magnetic Hydrogel Nanocomposites for Remote Controlled Pulsatile Drug Release. *J. Controlled Release* **2008**, *130*, 246−251.
(17) Mi, P.; Ju, X. J.; Xie, R.; Wu, H. G.; Ma, J.; Chu, L. Y. A Novel Stimuli-Responsive Hydrogel for K+-Induced Controlled-Release. *Polymer* **2010**, *51*, 1648−1653.
(18) Jeon, S. J.; Hauser, A. W.; Hayward, R. C. Shape-Morphing Materials from Stimuli-Responsive Hydrogel Hybrids. *Acc. Chem. Res.* **2017**, *50*, 161−169.
(19) Jeon, S. J.; Hayward, R. C. Reconfigurable Microscale Frameworks from Concatenated Helices with Controlled Chirality. *Adv. Mater.* **2017**, *29*, 1606111.
(20) Zhang, H.; Mourran, A.; Möller, M. Dynamic Switching of Helical Microgel Ribbons. *Nano Lett.* **2017**, *17*, 2010−2014.
(21) Huang, H. W.; Sakar, M. S.; Petruska, A. J.; Pane, S.; Nelson, B. J. Soft Micromachines with Programmable Motility and Morphology. *Nat. Commun.* **2016**, *7*, 12263.
(22) Na, J. H.; Evans, A. A.; Bae, J.; Chiappelli, M. C.; Santangelo, C. D.; Lang, R. J.; Hull, T. C.; Hayward, R. C. Programming Reversibly Self-Folding Origami with Micropatterned Photo-Crosslinkable Polymer Trilayers. *Adv. Mater.* **2015**, *27*, 79−85.
(23) Mourran, A.; Zhang, H.; Vinokur, R.; Möller, M. Soft Microrobots Employing Nonequilibrium Actuation *via* Plasmonic Heating. *Adv. Mater.* **2017**, *29*, 1604825.
(24) Lao, Z.; Zheng, Y.; Dai, Y.; Hu, Y.; Ni, J.; Ji, S.; Cai, Z.; Smith, Z. J.; Li, J.; Zhang, L.; et al. Nanogap Plasmonic Structures Fabricated by Switchable Capillary-Force Driven Self-Assembly for Localized Sensing of Anticancer Medicines with Microfluidic SERS. *Adv. Funct. Mater.* **2020**, 1909467.
(25) Kawata, S.; Sun, H. B.; Tanaka, T.; Takada, K. Finer Features for Functional Microdevices. *Nature* **2001**, *412*, 697−698.
(26) Hu, Y.; Wang, Z.; Jin, D.; Zhang, C.; Sun, R.; Li, Z.; Hu, K.; Ni, J.; Cai, Z.; Pan, D.; et al. Botanical-Inspired 4D Printing of Hydrogel at the Microscale. *Adv. Funct. Mater.* **2020**, *30*, 1907377.
(27) Zhang, Y. L.; Tian, Y.; Wang, H.; Ma, Z. C.; Han, D. D.; Niu, L. G.; Chen, Q. D.; Sun, H. B. Dual-3D Femtosecond Laser Nanofabrication Enables Dynamic Actuation. *ACS Nano* **2019**, *13*, 4041−4048.
(28) Yang, L.; Qian, D. D.; Xin, C.; Hu, Z. J.; Ji, S. Y.; Wu, D.; Hu, Y. L.; Li, J. W.; Huang, W. H.; Chu, J. R. Two-Photon Polymerization of Microstructures by a Non-Diffraction Multifoci Pattern Generated from a Superposed Bessel Beam. *Opt. Lett.* **2017**, *42*, 743−746.
(29) Cai, Z.; Liu, Y.; Zhang, C. C.; Xu, J. C.; Ji, S. Y.; Ni, J. C.; Li, J. W.; Hu, Y. L.; Wu, D.; Chu, J. R. Continuous Cubic Phase Microplates for Generating High-Quality Airy Beams with Strong Deflection. *Opt. Lett.* **2017**, *42*, 2483−2486.
(30) Ji, S. Y.; Yang, L.; Hu, Y. L.; Ni, J. C.; Du, W. Q.; Li, J. W.; Zhao, G.; Wu, D.; Chu, J. R. Dimension-Controllable Microtube Arrays by Dynamic Holographic Processing as 3D Yeast Culture Scaffolds for Asymmetrical Growth Regulation. *Small* **2017**, *13*, 1701190.
(31) Ji, S. Y.; Yang, L.; Zhang, C. C.; Cai, Z.; Hu, Y. L.; Li, J. W.; Wu, D.; Chu, J. R. High-Aspect-Ratio Microtubes with Variable Diameter and Uniform Wall Thickness by Compressing Bessel Hologram Phase Depth. *Opt. Lett.* **2018**, *43*, 3514−3517.
(32) Jin, D. D.; Chen, Q. Y.; Huang, T. Y.; Huang, J. Y.; Zhang, L.; Duan, H. L. Four-Dimensional Direct Laser Writing of Reconfigurable Compound Micromachines. *Mater. Today* **2020**, *32*, 19−25.
(33) Li, X.; Cai, X.; Gao, Y.; Serpe, M. J. Reversible Bidirectional Bending of Hydrogel-Based Bilayer Actuators. *J. Mater. Chem. B* **2017**, *5*, 2804−2812.
(34) Li, H.; Go, G.; Ko, S. Y.; Park, J. O.; Park, S. Magnetic Actuated pH-Responsive Hydrogel-Based Soft Micro-Robot for Targeted Drug Delivery. *Smart Mater. Struct.* **2016**, *25*, 027001.
(35) Malachowski, K.; Jamal, M.; Jin, Q.; Polat, B.; Morris, C. J.; Gracias, D. H. Self-Folding Single Cell Grippers. *Nano Lett.* **2014**, *14*, 4164−4170.
(36) Cools, J.; Jin, Q.; Yoon, E.; Alba Burbano, D.; Luo, Z.; Cuypers, D.; Callewaert, G.; Braeken, D.; Gracias, D. H. A Micropatterned Multielectrode Shell for 3D Spatiotemporal Recording from Live Cells. *Adv. Sci.* **2018**, *5*, 1700731.

https://dx.doi.org/10.1021/acsnano.0c00381
ACS Nano 2020, 14, 5233−5242

(37) Xu, W.; Paidi, S. K.; Qin, Z.; Huang, Q.; Yu, C. H.; Pagaduan, J. V.; Buehler, M. J.; Barman, I.; Gracias, D. H. Self-Folding Hybrid Graphene Skin for 3D Biosensing. *Nano Lett.* **2019**, *19*, 1409−1417.
(38) Cao, Y. Y.; Takeyasu, N.; Tanaka, T.; Duan, X. M.; Kawata, S. 3D Metallic Nanostructure Fabrication by Surfactant-Assisted Multiphoton-Induced Reduction. *Small* **2009**, *5*, 1144−1148.
(39) Xu, B. B.; Xia, H.; Niu, L. G.; Zhang, Y. L.; Sun, K.; Chen, Q. D.; Xu, Y.; Lv, Z. Q.; Li, Z. H.; Misawa, H.; et al. Flexible Nanowiring of Metal on Nonplanar Substrates by Femtosecond-Laser-Induced Electroless Plating. *Small* **2010**, *6*, 1762−1766.

https://dx.doi.org/10.1021/acsnano.0c00381
ACS Nano 2020, 14, 5233−5242